Design & Simulation of Robust H_∞ Control Based Power System Stabilizer for SMIB models

Jayapal R[†], **Dr. J.K.Mendiratta** [††],

[†] Research Scholar (VTU, Belgaum) & Assistant Professor, Electrical & Electronics Engg. Dept., R.V. College of Engg., Bengaluru-59, Karnataka, India.

[††] Professor, C.M.R. Institute of Tech., Bengaluru, ECE Dept., Karnataka, India.

Summary

This paper presents the design of a H_∞ control based power system stabilizer for a single machine infinite bus system when certain faults take place in a power system. The conventional power system stabilizer (CPSS) is bound to a particular operating state and its performance degrades when any deviation occurs from the quiescent operating state. Two power system models are considered herewith, viz., model 1.1 & model 2.2. In this context, a robust power system stabilizer (RPSS) is designed using the Glover-McFarlane's H_∞ loop shaping design procedure for a single machine infinite bus system & this concept is presented in this research paper. Guidance for loop shaping and synthesis of the robust controller are also presented along with the selection of the weighting functions. The resulting RPSS ensures the stability for a set of perturbed operating points with respect to the nominal system and has good oscillation damping ability. Comparisons are also made between the CPSS & RPSS. Various parameters such as the terminal voltage, torque, omega, rotor angle are plotted. The simulation results shown depict the effectiveness of the method developed for an SMIB based power system using the concept of robustness & H_∞ control.

Key words **:**

Robust controller, *Loop Shaping*, H_∞ *Synthesis*, *Glover-McFarlane Loop Shaping*, *Power System Modeling*, *SMIB*, *Power system stabilizer*.

1. Introduction

Power system stabilizers (PSS) have been used for many years to add damping to electromechanical oscillations. The use of fast acting high gain AVR's and the evolution of large interconnected power systems with transfer of bulk power across weak transmission links have further aggravated the problem of low frequency oscillations [17]. The continuous change in the operating condition and network parameters result in corresponding changes in the system dynamics [10]. This constantly changing nature of power systems makes the design of damping controllers a very difficult task. Power system stabilizers (PSS) were developed to extend stability limits by modulating the generator excitation to provide additional damping to the oscillations of synchronous machine rotors [8]. Recent developments in the field of robust control provide methods for designing fixed parameter controllers for systems subject to model uncertainties.

The robust PSS has the ability to maintain stability and achieve desired performance while being insensitive to the perturbations. Among the various robustness techniques, H_∞ optimal control [2] – [6] and the structured singular value (SSV or μ) technique have received considerable attention. But, the application of μ technique for controller design is complicated due to the computational requirements of μ design. Besides the high order of the resulting controller, also introduces difficulties with regard to implementation [11]. The H_∞ optimal controller design is relatively simpler than the μ synthesis in terms of the computational burden. This paper uses the Glover-McFarlane H_∞ loop shaping design procedure [1] to design the PSS. It combines the H_∞ robust stabilization with the classical loop shaping technique. The loop shaping is done without explicit regard to the nominal plant phase information.

A well-known method for the design of robust multiple input multiple-output (MIMO) feedback controllers is the so-called "H_∞ loop-shaping design procedure" proposed by McFarlane and Glover in [1]. This method has been successfully used in a variety of applications by various researchers in [15] & [16]. A full tutorial on how to design robust controllers using the H_∞ loop-shaping design procedure can be found in McFarlane and Glover [14] and Papageorgiou and Glover [13]. Even though designers usually obtain good loop-shaping weights (W) and controllers using their engineering insight and intuition, it is well recognized in the practicing community that the design of loop-shaping weights W_1 and W_2 to achieve a

Manuscript received November 5, 2009
Manuscript revised November 20, 2009

desired loop-shape is not always straightforward, especially for plants with strong cross-coupling [15] between them. This is because, it is not always clear how each element in the weights affects the singular values of the scaled nominal plant P and the complexity of this relationship considerably increases when non-diagonal weights need to be used. Also, the adhoc techniques (or trial and error methods) typically employed can be fairly time-consuming and can never be guaranteed to yield the best possible results. In the research work presented in this paper, we introduce this design procedure to PSS design for a single machine system and provide some basic guidelines for loop shaping weighting selection and controller design paradigm formulation.

The paper is organized in the following sequence as follows. A brief introduction about the background literature related to the H_∞ robust stabilization, Power systems stabilizers, etc. was presented in the previous paragraphs in the introductory section. The section 2 gives a brief overview of the H_∞ loop shaping technique employed along with the robust stabilization & the feedback controllers. Modeling of the power system with the design of the controllers & the simulation results is dealt with in section 3. Conclusions are presented in the fourth section followed by the nomenclature & the references with the author biographies.

2. H_∞ loop shaping design

The Glover-McFarlane H_∞ loop shaping design procedure [1], [16] consists of three steps, viz.,

- Loop shaping,
- Robust stabilization &
- Design of the final feedback controller.

All the 3 steps are briefly discussed as follows.

2.1 Loop Shaping

In loop shaping design, the closed-loop performance is specified in terms of requirements on the open-loop singular values. The open loop singular values are then shaped to give desired high or low gain at frequencies of interest. This step takes advantage of the conventional loop shaping technique, but no phase requirements need to be considered. That is, the closed-loop stability requirements are disregarded since the H_∞ synthesis step taken thereafter will robustly stabilize the shaped plant. Using a pre-compensator W_1 and or a post-compensator W_2, the singular values of the nominal plant are shaped to give a desired open-loop shape. W_1 is selected to keep the sensitivity

$$S = (I + GK)^{-1} \tag{1}$$

low at low frequencies such that

$$\left\| W_1^{-1} S \right\|_\infty \le 1, \tag{2}$$

while W_2 is selected to keep the complementary sensitivity

$$T = GK\,(I + GK)^{-1} \tag{3}$$

low at high frequencies such that

$$\left\| W_2^{-1} T \right\|_\infty \le 1. \tag{4}$$

This ensures acceptable level of performance as well as stability in the face of perturbations. The nominal plant G and shaping functions W_1, W_2 are combined to form shaped plant,

$$G_s = W_2 G W_1. \tag{5}$$

2.2 Robust stabilization

It has been shown that the largest achievable stability margin $\varepsilon_{\max}$ can be obtained by a non-iterative method [4], [1]. Here, $\varepsilon_{\max,}$ is the stability margin for the normalized co-prime factor robust stability problem [1]. It provides a robust stability guarantee for the closed loop system. Suppose $\overline{M}_s, \overline{N}_s$, are normalized left co-prime factors of G_s such that

$$G_s = \overline{M}_s^{-1} \overline{N}_s, \tag{6}$$

then,

$$e_{\max} = \left(1 - \left\| [\overline{M_s} . \overline{N_s}] \right\|_{\mathrm{H}}^2 \right)^{1/2}, \tag{7}$$

where, $\|\cdot\|_{\mathrm{H}}$ denotes the Hankel norm.

The controller is now defined by selecting $\varepsilon <= \varepsilon_{\max}$ and then synthesizing a stabilizing controller K_∞, which satisfies

$$\left\| \begin{bmatrix} \mathrm{I} \\ \mathrm{K}_\infty \end{bmatrix} (\mathrm{I} - Gs\mathrm{K}_\infty)^{-1} \overline{\mathrm{M}}_s^{-1} \right\|_\infty \le \varepsilon^{-1} \tag{8}$$

as shown in the Fig. 1.

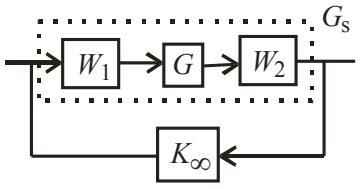

Fig. 1 : Block diagram of the synthesis of a stabilizing controller

The $\|\cdot\|_\infty$ denotes the H_∞ norm which is the supremum of the largest singular value over all frequencies. If $\varepsilon_{\max} << 1$, then return to the section 2.1 and adjust W_1 and W_2.

2.3 The Final Feedback Controller

The final feedback controller K is then constructed by combining the H_∞ controller K_∞ with the shaping functions W_1 and W_2 such that $K = W_1 K_\infty W_2$ as shown in Fig. 2.

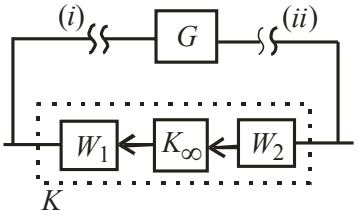

Fig. 2 : Block diagram of the final feedback controller K

3. Modelling & control of power systems with PSS

The power system stabilizer design for any power system to start with requires a mathematical model. To study the control of power system oscillations, single-machine system connected to infinite bus through a transmission line, taken from [9] is used. Two models of synchronous machine are considered to test the performance of the designed RPSS. Modeling, synthesizing controller and simulation are performed independently for both the models, viz., the model 1.1 & model 2.2. Each model is being treated as a separate case in sub-sections 3.1 & 3.2 & finally the results of the 2 models are compared with the CPSS & RPSS. To start with, the model 1.1 is discussed, followed by the model 2.2.

3.1 Model 1.1

In this section, the model of the power system for the model 1.1 is presented along with the brief design of the robust controller. The eigen value analysis also presented along with the simulation results & the discussions on it.

3.1.1 Modelling of power system model 1.1

The single line diagram (SLD) shown in the Fig. 3 represents the SMIB based power system, wherein the generator is represented by the Model 1.1 [9]. In this model 1.1, one field winding on d-axis and one equivalent damper on q-axis are considered. The relevant equations of model 1.1 is given in the following equations Eqns. 9 to 32 respectively [9]. The data for this power system model 1.1 is given as Data I below.

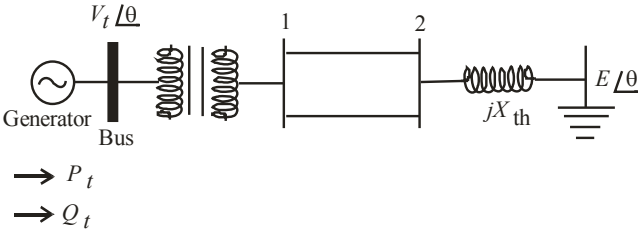

Fig. 3 : SMIB power system using the model 1.1.

DATA I : The system data corresponding to the Model 1.1 (Fig. 3) on a 1000 MVA base (in p.u.) is

Generator :

$R_a = 0.00327$, $x_d = 1.7572$, $x_q = 1.5845$, $x'_d = 0.424$, $x'_q = 1.04$, $T'_{d0} = 6.660$, $T'_{q0} = 0.44$, $H = 3.542$, $f_B = 50$ Hz.

Transformer :

$R_t = 0.0$, $x_t = 0.1364$.

Transmission Line (per circuit) :

$R_l = 0.08593$, $X_L = 0.8125$, $B_c = 0.1184$.

Excitation system :

$K_a = 400$, $T_a = 0.025$, $E_{f\,dmax} = 6.0$, $E_{fdmin} = -6.0$.

Operating Data :

$E_b = 1.0$, $P_t = 0.6$, $Q_t = 0.02224$, $V_t = 1.05$ V, $\theta = 21.65$, $X_{th} = 0.13636$.

The mathematical model of the power system is required to design any type of controller. This mathematical model may be in the form of a differential equation or in transfer function form or in state space form. The system equations of the SMIB based power system corresponding to Model 1.1 are as shown below [9].

$$\frac{d\delta}{dt} = \omega'_B\left(S_m - S_{mo}\right), \tag{9}$$

$$\frac{dS_m}{dt} = \frac{1}{2H}\left[-D\left(S_m - S_{mo}\right) + T_m - T_e\right], \tag{10}$$

$$\frac{dE'_q}{dt} = \frac{1}{T'_{d0}}\left[-E'_q + \left(x_d - x'_d\right)i_d + E_{fd}\right], \tag{11}$$

$$\frac{dE'_d}{dt} = \frac{1}{T'_{q0}}\left[-E'_d - \left(x_q - x'_q\right)i_q\right], \tag{12}$$

$$\frac{dE_{fd}}{dt} = \frac{1}{T_A}\left[K_A\left(V_{ref} - V_t\right)\right] - \frac{1}{T_A}E_{fd}\,. \tag{13}$$

The first two equations are obtained from the second order swing equation as

$$M\frac{d^2\delta}{dt^2} + D'\frac{d\delta}{dt} = T_m - T_e\,, \tag{14}$$

$$M = \frac{2H}{\omega_B}\,. \tag{15}$$

The stator equations in *dq* & DQ reference frames are given as

$$E'_q + x'_d i_d - R_a i_q = v_q \tag{16}$$

and

$$E'_d - x'_q i_q - R_a i_d = v_d . \tag{17}$$

If

$$x'_d = x'_q = x', \tag{18}$$

then

$$\left(E'_q + jE'_d\right) - \left(R_a + jx'\right)\left(i_q + ji_d\right) = \left(v_q + jv_d\right) \tag{19}$$

or

$$\left(E'_Q + jE'_D\right) - \left(R_a + jx'\right)\left(i_Q + ji_D\right) = \left(v_Q + jv_D\right) \tag{20}$$

The system equations such as the torque, state variable equations are also presented here in this context. The electrical torque, T_e is expressed in terms of state variables E'_d & E'_q and the non-state variables i_d & i_q and is expressed as

$$T_e = E'_d i_d + E'_q i_q + \left(x'_d - x'_q\right) i_d i_q . \tag{21}$$

The direct axis & quadrature axis currents in the synchronous machine, i_d & i_q can be obtained from the following linear equations as

$$\begin{bmatrix} (x'_d + z_I) & -(R_a + z_R) \\ -(R_a + z_R) & -(x'_q + z_I) \end{bmatrix} \begin{bmatrix} i_d \\ i_q \end{bmatrix} = \begin{bmatrix} h_1 E_b \cos\delta + h_2 E_b \sin\delta - E'_q \\ h_2 E_b \cos\delta - h_1 E_b \sin\delta - E'_d \end{bmatrix} . \tag{22}$$

Here, in the above equation, ($z_R + j\ z_I$) is the input impedance of the external network viewed from the generator terminals with infinite bus shorted. ($h_1 + jh_2$) is the voltage gain at the terminals with armature open circuited [9].

The initial conditions for the system equations for P_{to}, Q_{to}, V_{to} and θ_0 are obtained from the power flow analysis in steady state as

$$I_{ao}\angle\phi_o = \frac{P - jQ_{to}}{V_{to}\angle -\theta_o}, \tag{23}$$

$$E_{qo}\angle\delta_o = V_{to}\angle\theta_o + (R_a + jx_q) I_{ao}\angle\phi_o , \tag{24}$$

$$i_{do} = -I_{ao}\sin(\delta_o - \phi_o), \tag{25}$$

$$i_{qo} = I_{ao}\cos(\delta_o - \phi_o), \tag{26}$$

$$v_{do} = -V_{to}\sin(\delta_o - \theta_o), \tag{27}$$

$$v_{qo} = V_{to}\cos(\delta_o - \theta_o), \tag{28}$$

$$E_{fdo} = E_{qo} - (x_d - x_q) i_{do}, \tag{29}$$

$$E'_{qo} = E_{fdo} + (x_d - x'_d) i_{do}, \tag{30}$$

$$E'_{do} = -(x_q - x'_q) i_{qo}, \tag{31}$$

$$T_{eo} = E'_{qo} i_{qo} + E'_d i_{do} + (x'_d - x'_q) i_{do} i_{qo} = T_{mo} . \tag{32}$$

The model is simulated & the linearized model is finally obtained, which is further used for the controller design.

3.1.2 Controller design for the model 1.1

To start with, the design of the conventional power system stabilizer is presented. The schematic representation of Conventional Power System Stabilizer (CPSS) is as shown in the Fig. 4.

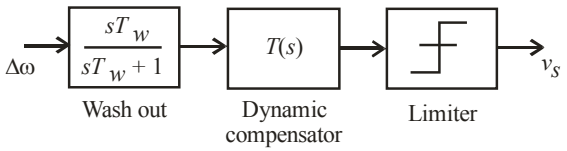

Fig. 4 : Conventional Power system Stabilizer

In the block diagram of the CPSS shown, the transfer function $T(s)$ is finally obtained as

$$T(s) = \frac{Ks(1 + sT_1)(1 + sT_3)}{(1 + sT_2)(1 + sT_4)} . \tag{33}$$

The designed parameters of CPSS for the above system [9] are taken as

$K_s = 15,\ T_1 = 0.75\,s,\ T_2 = 0.3\,s,\ T_w = 10,$

limits on V_s as $+0.05$ & -0.05.

Now, we proceed forward to the design of the robust controller for the model 1.1. The H_∞ loop shaping design procedure is applied as shown in Figs. 1 & 2. The shaping objective is to make the output $y = \Delta\omega$ (the generator frequency variation) as small as possible with disturbance signal $d = \Delta V_{ref}$. Since the frequency of the intra-plant mode is around 3 rad / s, the performance objective has been translated to increase the open-loop gain around that frequency. After that, an H_∞ controller ; K_∞, was synthesized to ensure the robust stability of the closed-loop system. Finally, K_∞ was cascaded with the shaping functions to form the final controller $K = w_1\, K_\infty\, W_2$.

The selection of the weight W_1 for the H_∞ control purposes is done as follows. We add pole and zero pairs to achieve increase in gain in the desired frequency range, while keeping the gain change as small as possible around other frequencies [16]. The system has poor damping at frequencies $1/0.1603$ and at $1/0.035$. Hence, gain has to be improved at these frequencies. A washout filter block in W_1 with time constant 10 *s* is used to ensure the controller only works in the transient state [10].

The resulting transfer function for the weighting W_1 is obtained as

$$\frac{17682*10s*(1+0.33s)}{(1+10s)(1+0.1603s)(1+0.035)}. \quad (34)$$

The selection of the weight W_2 for the H_∞ control purposes is done as follows. To increase the gain of the system at low frequency, 3 repeated zeros are added at 30. To make W_2 proper and to achieve proper slope of G_s at cross over frequency 3 poles are added at insignificant frequency of 10000. The reduced DC gain of W_2 is compensated by using a constant 10^4. The resulting transfer function for the weighting W_2 is obtained as

$$\frac{10^4*(s+30)^3}{(s+10000)^3}. \quad (35)$$

The resulting singular value plot of nominal system G, W_1, W_2 and resulting shaped plant G_s due to the reference voltage variation to the generator frequency variation are as shown in Fig. 5.

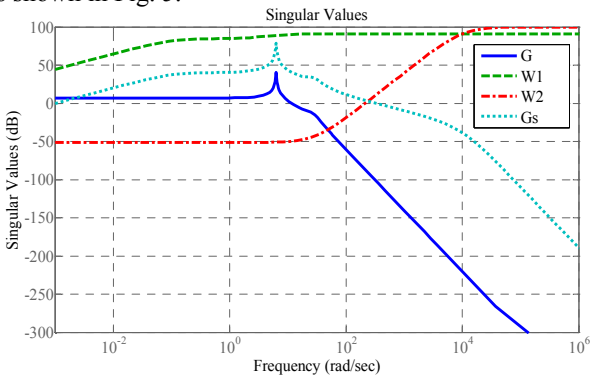

Fig. 5: Singular value plot of nominal system G, W_1, W_2 & G_s

In this context, we present the H_∞ synthesis. We synthesize a K_∞ controller to achieve robust stability for the nominal plant. The maximum stability margin is $\varepsilon_{max} = 0.6316$. This margin evaluates the feasibility of our loop shaping design. The objective function for the H_∞ robust stabilization is

$$\left\| \begin{bmatrix} I \\ K_\infty \end{bmatrix} (I - GsK_\infty)^{-1} M_s^{-1} \right\|_\infty \le 0.6316^{-1}. \quad (36)$$

According to McFarlane and Glover [1], given the normalized left co-prime factorization of the nominal plant as

$$G_{s_0} = \overline{M}_s^{-1} N_s, \quad (37)$$

the controller K_∞ can stabilize all

$$G_s = \left(\overline{M} + \Delta_M\right)^{-1} \left(\overline{N} + \Delta_N\right) \quad (38)$$

satisfying

$$\left\|\Delta_M, \Delta_N\right\|_\infty < 0.6316. \quad (39)$$

Thus, in terms of the gap metric, all G_s with

$$\delta_g\left(G_s, G_{s_0}\right) < 0.6316 \quad (40)$$

can be stabilized by this controller [1].

The final controller K is designed as follows. The resulting controller has a high order of 14. The controller is reduced to a 7^{th} order controller using the Hankel Norm reduction [11] method. The transfer function of the reduced order controller is given as

$$G_k(s) = \frac{N(s)}{D(s)}, \quad (41)$$

with

$$\begin{aligned} N(s) = {} & 4.317\times10^9 s^7 + 7.261\times10^{13} s^6 + \\ & 3.199\times10^{17} s^5 + 3.89\times10^{19} s^4 + \\ & 1.666\times10^{21} s^3 + 3.397\times10^{22} s^2 \\ & + 1.951\times10^{23} s + 1.231\times10^{22} \end{aligned} \quad (42)$$

$$\begin{aligned} D(s) = {} & s^7 + 4.737\times10^4 s^6 + 9.048\times10^8 s^5 + \\ & 8.773\times10^{12} s^4 + 4.336\times10^{16} s^3 + \\ & 8.8094\times10^{19} s^2 + 3.924\times10^{21} s + \\ & 1.235\times10^{22} \end{aligned} \quad (43)$$

The bode plots of the full-order controller and the reduced-order controller is shown in Fig. 6.

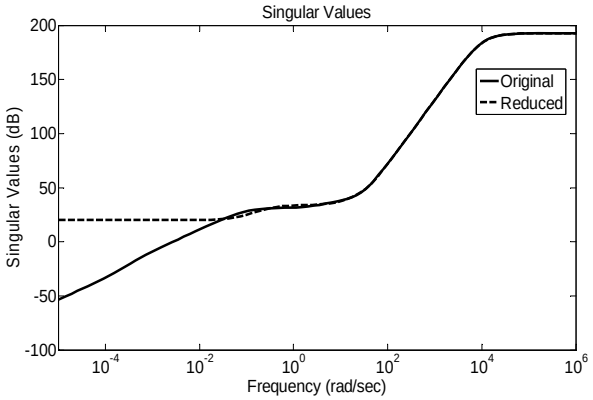

Fig. 6 : Bode plot of the full-order controller and the reduced-order controller for model 1.1.

3.1.3 Development of the simulink model for the power system model 1.1 in Matlab

The model of the power system was developed using the power system, power electronics, control system, signal processing toolboxes & from the basic functions available in the Simulink library in Matlab / Simulink. The initial conditions are calculated and model is created using

simulink in Matlab. In this paper, plots of terminal voltages, rotor angle, electric torque, omega, etc are plotted as functions of time with RPSS & CPSS and the waveforms are observed on the scopes. The entire system modeled in Simulink is a closed loop feedback control system consisting of the plants, controllers, comparators, feedback systems, the mux, de-mux, summers, adders, gain blocks, integrators, state-space models, sub-systems, the output sinks (scopes) & the input sources. The developed simulink model with CPSS & RPSS for the power system model 1.1 is shown in the Figs. 7 & 8 respectively.

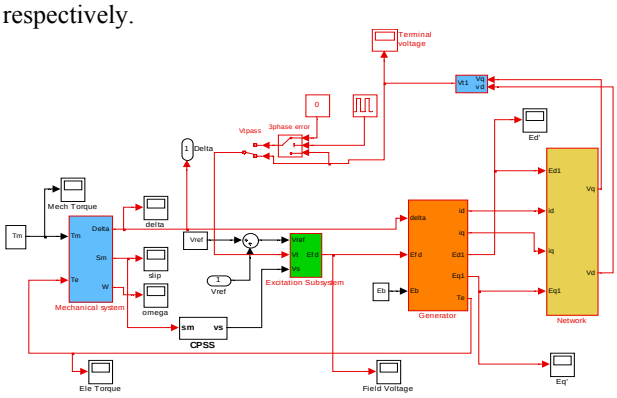

Fig. 7 : The developed simulink model with CPSS & control for the power system model 1.1.

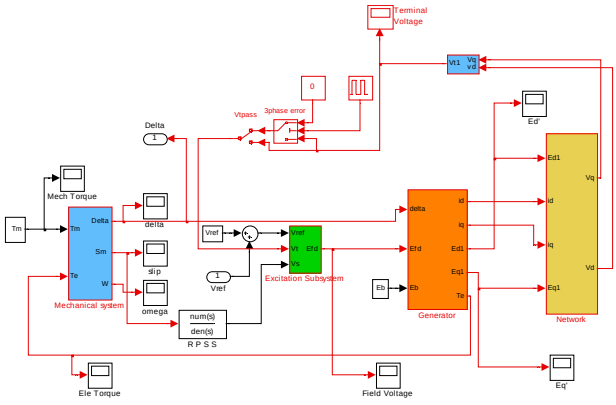

Fig. 8 : The developed simulink model with RPSS & control for the power system model 1.1.

3.1.4 Eigen Value analysis of Model 1.1

The eigen value analysis is also performed for the model 1.1 without the PSS & the values are obtained as –73.9756, –8.2488 ± *i* 27.3754, –0.0618 ± *i* 6.2356, –2.7038 & the corresponding response is as shown in the Fig. 9.

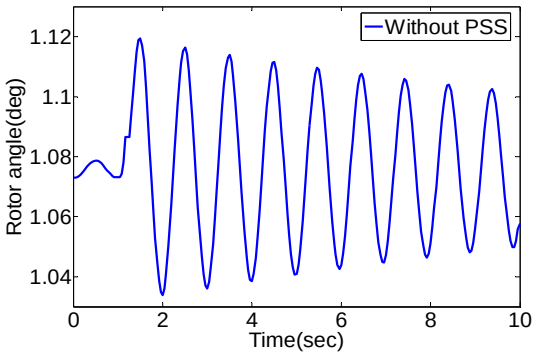

Fig. 9 : Response off rotor angle without PSS

The eigen value analysis is also performed for the model 1.1 with the CPSS & the values are obtained as –103.04, –71.53, –7.2103 ± *i* 29.484, –0.81365 ± *i* 5.8377, –0.10042, –2.6841 & the corresponding response is as shown in the Fig. 10.

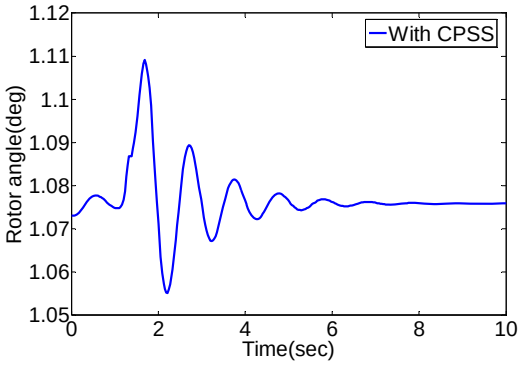

Fig. 10 : Response of rotor angle with CPSS

The eigen value analysis is also performed for the model 1.1 with the RPSS & the values are obtained as –21088, –4759.6 ± *i* 9756.1, –8348.7 ± *i* 1537.5, –71.505, –46.404, –16.651 ± *i* 27.436, –0.35172, –2.4375 ± *i* 3.0283, –2.4315 & the corresponding response is as shown in the Fig.11.

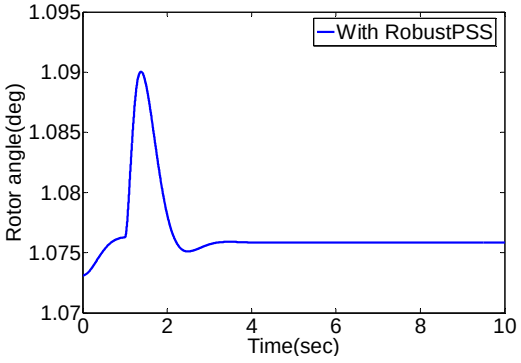

Fig. 11 : Response off Rotor angle with RPSS

3.1.5 Simulation results & discussions

Simulations are performed using the developed simulink model shown in the Figs. 7 & 8 for a period of 10 secs with the designed CPSS & RPSS and the results are observed, which are presented in Figs. 12 - 15 respectively. The non-linear simulations are performed, *for extreme fault conditions,* using simulink to test the efficiency of the designed controller. 4 different types of faults were considered as case A, B, C & D respectively.

Case A :

$P_t = 0.6,\ Q_t = 0.02224,\ V_{ref} = 2.2\,(\text{for } 0.1\,s),\ T_m = 1.0$

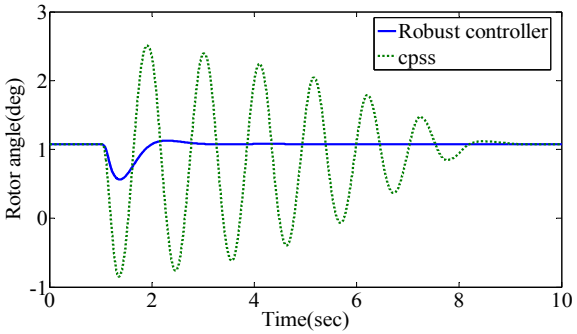

Fig. 12 : Plot of variation of rotor angle vs. time

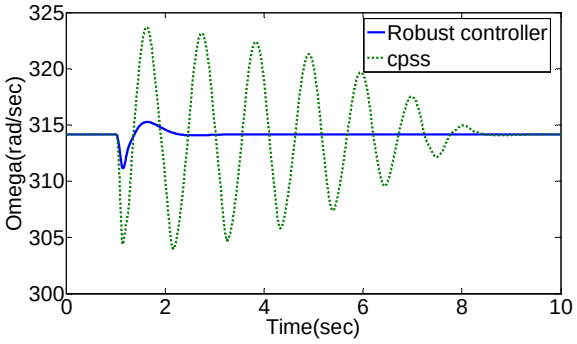

Fig. 13 : Plot of omega vs. time

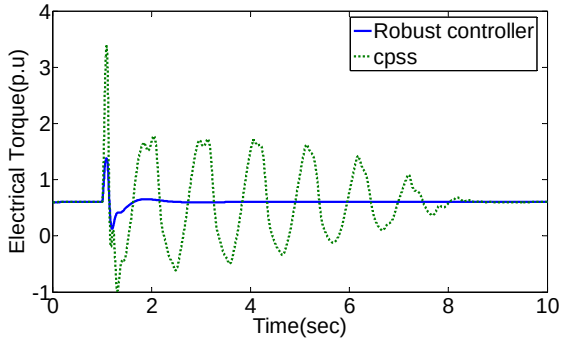

Fig. 14 : Plot of electrical torque vs. time

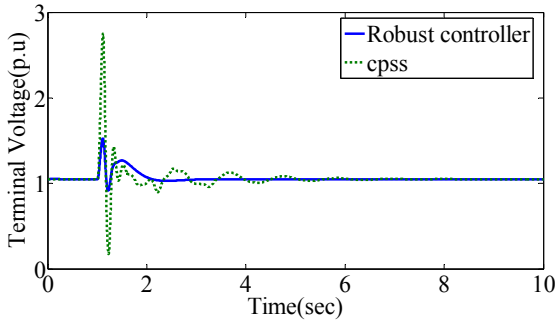

Fig. 15 : Plot of terminal voltage vs. time

From the Figs. 12 to 15, it can be clearly seen that system with RPSS, the settling time and deviation in magnitudes during transients are insignificant & consistent when compared to the CPSS. The quantitative results of the comparison of the settling times of the various parameters with CPSS & RPSS is shown in the table 1.

Parameter	Settling time (secs)	
	CPSS	RPSS
Rotor angle	10	3
Omega	10	3
Torque	10	3
Voltage	10	3

Table 1 : Quantitative results of the settling times of different parameters with CPSS & RPSS for the model 1.1.

In addition to the above fault as mentioned in case A, three more cases are simulated, namely

Case B :

$P_t = 0.6,\ Q_t = 0.02224,\ V_{ref} = 1.0,\ T_m = 2.5\,(\text{for } 0.1\,s)$

Case C :

$P_t = 0.6 \times 2,\ Q_t = 0.02224 \times 2,\ V_{ref} = 1.0,\ T_m = 1.0$

Case D : Three phase fault for 0.08 sec.

The simulation results of all these cases are similar to the results shown for case A.

For justification of robustness, the following four cases with step changes in the reference voltages are considered, namely,

Case 1: $V_{ref} \times 1.0$

Case 2: $V_{ref} \times 2.0$

Case 3: $V_{ref} \times 2.3$

Case 4: $V_{ref} \times 3.0$

The simulation results corresponding to the above 4 cases are shown in the Figs. 16 to 23 respectively. The results shown in Figs. 16, 18, 20 & 22 correspond to the system with RPSS while the results shown in Figs.17, 19, 21 & 23 respectively correspond to the system with CPSS.

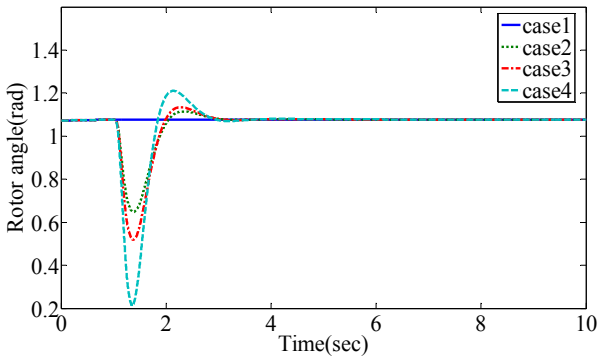

Fig. 16 : Plot of rotor angle vs. time for the 4 cases

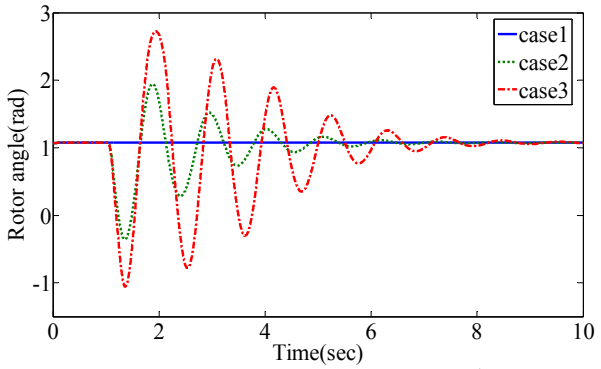

Fig. 17 : plot of rotor angle vs. time for the 1st 3 cases

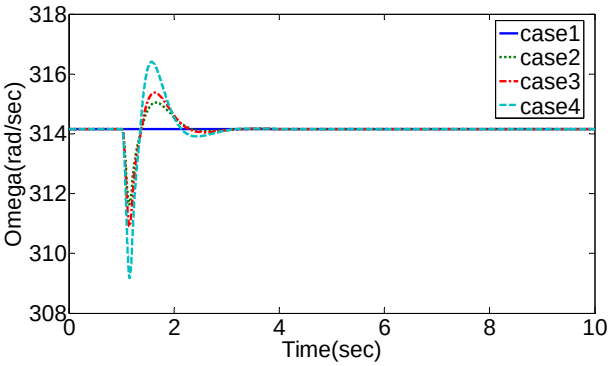

Fig. 18 : Plot of omega vs. time for the 4 cases

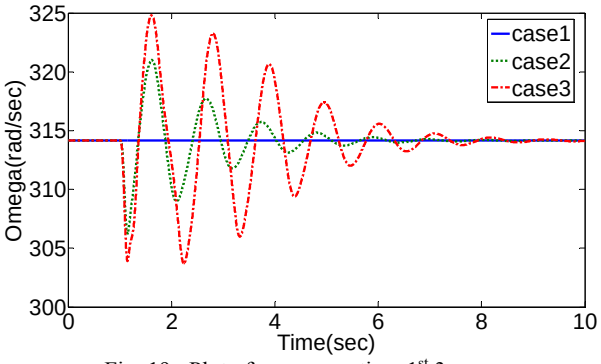

Fig. 19 : Plot of omega vs. time 1st 3 cases

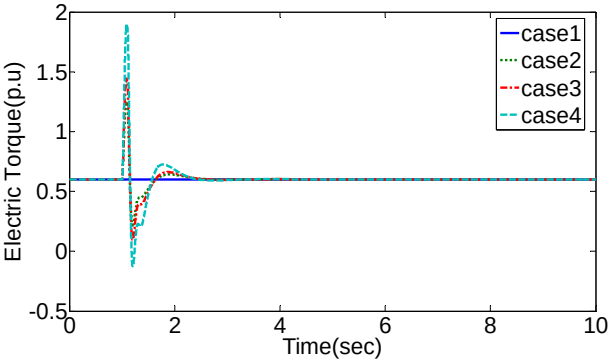

Fig. 20 : Plot of electrical torque vs. time for the 4 cases

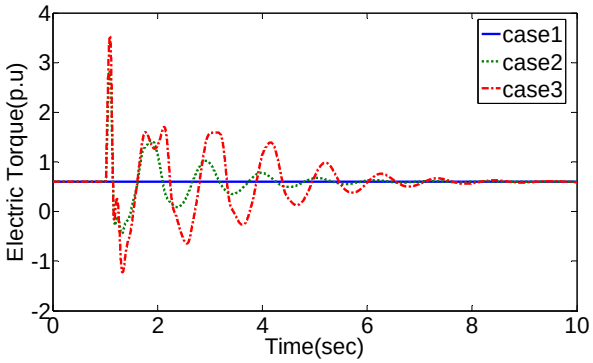

Fig. 21 : Plot of electrical torque vs. time for the 3 cases

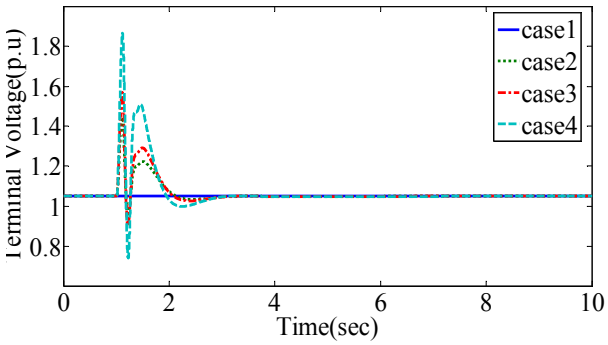

Fig. 22 : Plot of terminal voltage vs. time for the 4 cases

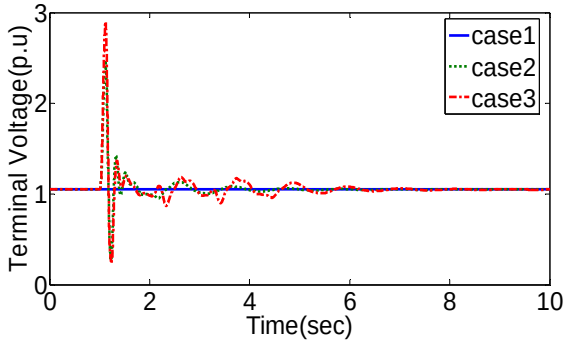

Fig. 23 : Plot of terminal voltage vs. time for the 1st 3 cases

From the above simulation results shown in the Figs. 16 - 23, it can be very clearly seen that the system with RPSS provides robustness, i.e., the variations in magnitudes and the settling times are almost independent of the type and magnitude of faults, while the system with CPSS fails to provide robustness as the settling time depends upon the type of faults, also the response characteristics for various parameters settle at a faster rate compared to the CPSS case, thus provide excellent damping. Also, in case of CPSS, the results are shown only for first three cases since the system with CPSS becomes unstable for the case 4.

3.2 Model 2.2

In this section, the model of the power system for the model 2.2 is presented along with the brief design of the robust controller. The eigen value analysis also presented along with the simulation results & the discussions on it.

3.2.1 Modelling of power system model 2.2

The single line diagram (SLD) shown in the Fig. 24 represents the SMIB based power system, wherein the generator is represented by the Model 2.2 [9]. In this model 2.2, one field winding, one equivalent damper winding on *d*-axis and two equivalent damper windings on *q*-axis are considered. The relevant equations of model 1.1 is given in the following equations Eqns. 44 to 62 respectively [9]. The data for this power system model 2.2 is given as Data II below.

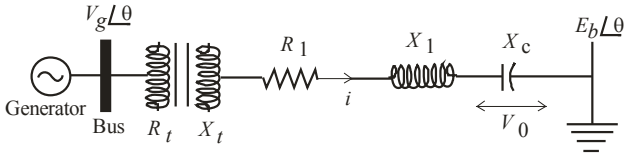

Fig. 24 : SMIB power system using the 2.2 model

Data II: The system data corresponding to the Model 2.2 (Fig. 19) on a 1000 MVA base (in p.u.) is

Generator :

$R_a = 0$, $x_d = 1.79$, $x_q = 1.71$, $x'_d = 0.169$, $x''_d = 0.135$, $x'_q = 0.228$, $x''_q = 0.2$, $T'_{do} = 0.4$, $D = 0$, $T''_{do} = 0.0259$, $T'_{qo} = 0.1073$, $T''_{qo} = 0.0463$, $H = 5$, $f_B = 60$ Hz.

Transformer :

$R_t = 0.0$, $x_t = 0.2$.

Transmission Line :

$R_l = 0.02$, $X_L = 0.8$, $X_c = 0.3$.

Excitation system :

$K_a = 200$, $T_a = 0.025$, $E_{fdmax} = 5.5$, $E_{fdmin} = -5.5$.

The mathematical model of the power system is required to design any type of controller. This mathematical model may be in the form of a differential equation or in transfer function form or in state space form. The system equations of the SMIB based power system corresponding to Model 2.2 are as shown below [9]:

The stator equations are modeled as

$$\frac{d\Psi_d}{dt} = -\omega\Psi_q - \omega_B R_a i_d - \omega_B v_d , \tag{44}$$

$$\frac{d\Psi_q}{dt} = -\omega\Psi_q - \omega_B R_a i_q - \omega_B v_q . \tag{45}$$

The rotor equations are modeled as

$$\frac{d\Psi_h}{dt} = \frac{1}{T''_d}\left[-\Psi_h + \Psi_d\right], \tag{46}$$

$$\frac{d\Psi_f}{dt} = \frac{1}{T'_d}\left[-\Psi_f + \Psi_d + \frac{x'_d}{x_d - x'_d} E_{fd}\right], \tag{47}$$

$$\frac{d\Psi_g}{dt} = \frac{1}{T''_q}\left[-\Psi_g + \Psi_q\right], \tag{48}$$

$$\frac{d\Psi_k}{dt} = \frac{1}{T''_q}\left[-\Psi_k + \Psi_d\right]. \tag{49}$$

The rotor mechanical equations are given by

$$\frac{d\delta}{dt} = \omega_b\left(S_m - S_{m0}\right), \tag{50}$$

$$2H\frac{dS_m}{dt} = -D\left(S_m - S_{m0}\right) + \left(T_m - T_e\right), \tag{51}$$

where

$$S_m = \frac{\omega - \omega_b}{\omega_b}, \quad S_{m0} = 0 . \tag{52}$$

The electrical torque equation is given by

$$T_e = \Psi_d i_d - \Psi_q i_q , \tag{53}$$

where

$$i_d = \frac{\Psi_d}{x''_d} - \frac{x'_d - x''_d}{x'_d x''_d}\Psi_h - \frac{x'_d - x''_d}{x'_d x''_d}\Psi_f , \tag{54}$$

$$i_q = \frac{\Psi_q}{x''_q} - \frac{x'_q - x''_q}{x'_q x''_q}\Psi_k - \frac{x'_q - x''_q}{x'_q x''_q}\Psi_g . \tag{55}$$

The final differential equation is given by

$$\frac{dV_R}{dt} = \frac{1}{T_a}\left[-V_R + K_a\left(V_{ref} + V_s - V_t\right)\right], \tag{56}$$

$$\frac{V'_t}{V_t} = \frac{1}{1 + sT_m} . \tag{57}$$

The network equation from the generator terminal to the infinite bus is given by

$$\begin{bmatrix} V_d \\ V_q \end{bmatrix} = \begin{bmatrix} R_E & -\omega x_E \\ -\omega x_E & R_E \end{bmatrix} \begin{bmatrix} i_d \\ i_q \end{bmatrix} + \frac{x_E}{\omega_b} \begin{bmatrix} di_d/dt \\ di_q/dt \end{bmatrix} + \begin{bmatrix} \cos\delta & \sin\delta \\ \sin\delta & \cos\delta \end{bmatrix} \left\{ \begin{bmatrix} V_{CD} \\ V_{CQ} \end{bmatrix} + \begin{bmatrix} 0 \\ 1 \end{bmatrix} E_b \right\}, \quad (58)$$

where

$$\frac{di_d}{dt} = \frac{1}{x''_d}\frac{d\Psi_d}{dt} - \frac{x'_d - x''_d}{x'_d x''_d}\frac{d\Psi_h}{dt} - \frac{x'_d - x''_d}{x'_d x''_d}\frac{d\Psi_f}{dt}, \quad (59)$$

$$\frac{di_q}{dt} = \frac{1}{x''_q}\frac{d\Psi_q}{dt} - \frac{x'_q - x''_q}{x'_q x''_q}\frac{d\Psi_k}{dt} - \frac{x'_q - x''_q}{x'_q x''_q}\frac{d\Psi_g}{dt}. \quad (60)$$

The state equation in the dq form (series capacitor differential equations) is represented as

$$\frac{dV_{CD}}{dt} = \frac{\omega_b}{X_C} I_D - \omega_0 V_{CQ}, \quad (61)$$

$$\frac{dV_{CQ}}{dt} = \frac{\omega_b}{X_C} I_Q - \omega_0 V_{CD}. \quad (62)$$

3.2.2 Controller design for the model 2.2

To start with, the design of the conventional power system stabilizer is presented. The schematic representation of Conventional Power System Stabilizer (CPSS) is as shown in the Fig. 4. In the block diagram of the CPSS shown in the Fig. 4, the transfer function $T(s)$ is finally obtained as

$$T(s) = \frac{Ks(1+sT_1)(1+sT_3)}{(1+sT_2)(1+sT_{4)}}. \quad (63)$$

The designed parameters of CPSS for the above system [9] are taken as $K_s = 6$, $T_1 = 0.1s$, $T_2 = 0.01s$, $T_w = 10$, limits on $V_s = +0.1$ & -0.1.

Now, we proceed forward to the design of the robust controller for the model 2.2. The H_∞ loop shaping design procedure is applied as shown in Figs. 1 & 2 respectively. The shaping objective is to make the output $y = \Delta\omega$ (the generator frequency variation) as small as possible with disturbance signal $d = \Delta V_{ref}$. Since the frequency of the intra-plant mode is around 3 rad / s, the performance objective has been translated to increase the open-loop gain around that frequency. After that, an H_∞ controller ; K_∞, was synthesized to ensure the robust stability of the closed-loop system. Finally, K_∞ was cascaded with the shaping functions to form the final controller $K = w_1 K_\infty W_2$.

The selection of the weight W_1 for the H_∞ control purposes is done as follows. We add pole and zero pairs to achieve increase in gain in the desired frequency range, while keeping the gain change as small as possible around other frequencies [16]. The system has poor damping at frequencies $1/0.1595$ and at $1/0.0054$. Hence, gain has to be improved at these frequencies. A washout filter block in W_1 with time constant 10 s is used to ensure the controller only works in the transient state [10]. The resulting transfer function for the weighting W_1 is obtained as

$$\frac{17682 * 10s * (1+0.33s)}{(1+10s)(1+0.1595s)(1+0.0054)}. \quad (64)$$

The selection of the weight W_2 for the H_∞ control purposes is done as follows. To increase the gain of the system at low frequency, 3 repeated zeros are added at 90. To make W_2 proper and to achieve proper slope of G_s at cross over frequency 3 poles are added at insignificant frequency of 10000. The reduced DC gain of W_2 is compensated by using a constant 200. The resulting transfer function for the weighting W_2 is obtained as

$$\frac{200 * (s+90)^3}{(s+10000)^3}. \quad (65)$$

The resulting singular value plot of nominal system G, W_1, W_2 and resulting shaped plant G_s due to the reference voltage variation to the generator frequency variation are as shown in Fig. 25.

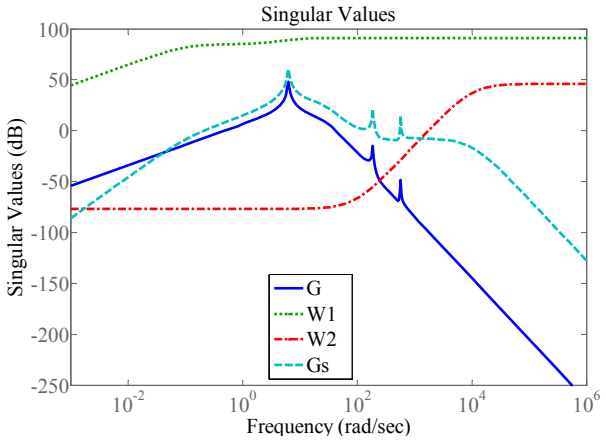

Fig. 25 : Singular value plot of nominal system G, W_1, W_2 and G_s

In this context, we present the H_∞ synthesis. We synthesize a K_∞ controller to achieve robust stability for the nominal plant. The maximum stability margin is $\varepsilon_{max} = 0.5680$. This margin evaluates the feasibility of our loop shaping design. The objective function for the H_∞ robust stabilization is

$$\left\| \begin{bmatrix} \mathrm{I} \\ \mathrm{K}_\infty \end{bmatrix} (\mathrm{I} - Gs\mathrm{K}_\infty)^{-1} \mathrm{M}_s^{-1} \right\|_\infty \le 0.5680^{-1}. \quad (66)$$

According to McFarlane and Glover [1], given the normalized left co-prime factorization of the nominal plant as

$$G_{s_0} = \overline{M}_s^{-1} N_s, \quad (67)$$

the controller K_∞ can stabilize all

$$G_s = \left(\overline{M} + \Delta_M\right)^{-1} \left(\overline{N} + \Delta_N\right) \quad (68)$$

satisfying

$$\left\|\Delta_{\mathrm{M}}, \Delta_{\mathrm{N}}\right\|_\infty < 0.5680. \quad (69)$$

Thus, in terms of the gap metric, all G_s with

$$\delta_g\left(G_s, G_{s_0}\right) < 0.5680 \quad (70)$$

can be stabilized by this controller [1]. The final controller K is designed as follows. The resulting controller has a high order of 14. The controller is reduced to a 7^{th} order controller using the Hankel Norm reduction [11] method. The transfer function of the reduced order controller is given as

$$G_k(s) = \frac{N(s)}{D(s)}, \quad (71)$$

with

$$\begin{aligned} N(s) = {} & 9.9\times10^{6}s^{7} + 1.412\times10^{11}s^{6} + \\ & 5.578\times10^{14}s^{5} + 7.657\times10^{15}s^{4} \\ & + 2.162\times10^{20}s^{3} + 1.165\times10^{22}s^{2} \\ & + 2.044\times10^{23}s + 3.117\times10^{26} \end{aligned} \quad (72)$$

$$\begin{aligned} D(s) = {} & s^{7} + 4.549\times10^{4}s^{6} + 8.394\times10^{8}s^{5} + \\ & 7.065\times10^{12}s^{4} + 2.652\times10^{16}s^{3} + \\ & 3.474\times10^{19}s^{2} + 3.928\times10^{22}s + \\ & 1.178\times10^{25} \end{aligned} \quad (73)$$

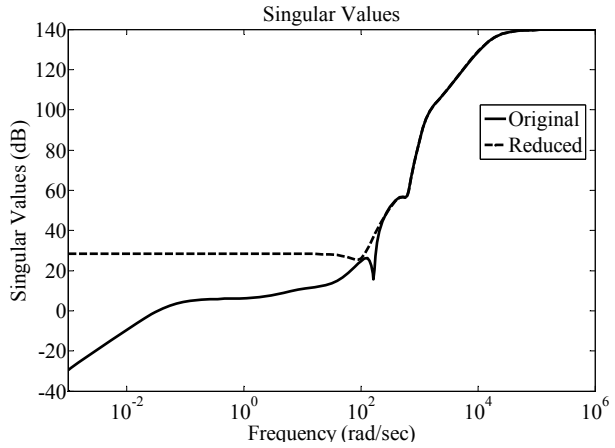

Fig. 26 : Original and reduced order controller for model 2.2

The bode plots of the full-order controller and the reduced-order controller is shown in Fig. 26.

3.2.3 Development of the simulink model for the power system model 1.1 in Matlab

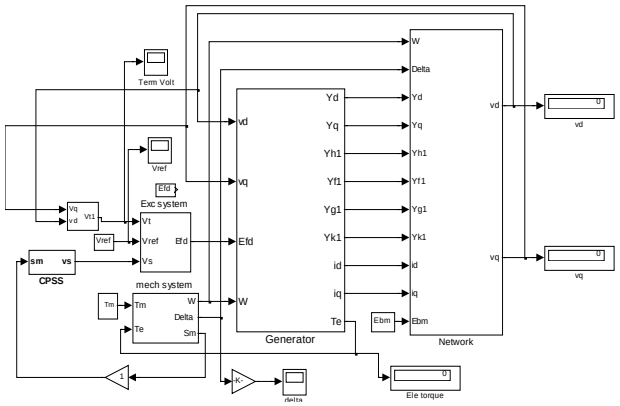

Fig. 27 : The developed simulink model with CPSS & control for the model 2.2.

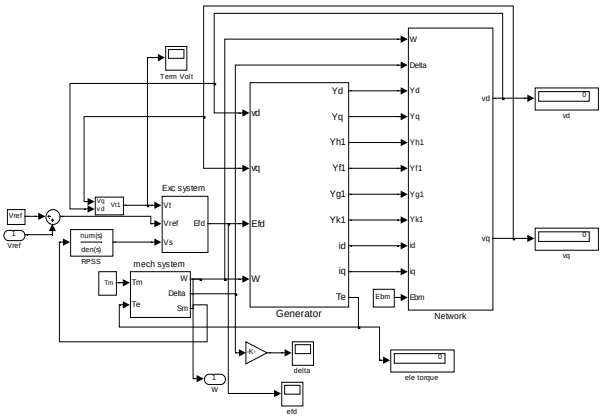

Fig. 28 : The developed simulink model with RPSS & control for the model 2.2.

The model of the power system was developed using the power system, power electronics, control system, signal processing toolboxes & from the basic functions available in the Simulink library in Matlab / Simulink. The initial conditions are calculated and model is created using simulink in Matlab. In this paper, plots of terminal voltages, rotor angle, electric torque, omega, etc are plotted as functions of time with RPSS & CPSS and the waveforms are observed on the scopes. The entire system modeled in Simulink is a closed loop feedback control system consisting of the plants, controllers, comparators, feedback systems, the mux, de-mux, summers, adders, gain blocks, integrators, state-space models, sub-systems, the output sinks (scopes) & the input sources. The

developed simulink model with CPSS & RPSS for the power system model 2.2 is shown in the Figs. 27 & 28 respectively.

3.2.4 : Eigen value analysis of model 2.2

The eigen value analysis is also performed for the model 2.2 without the PSS & the values are obtained as −3.4522 ± *i* 568.15, −499.2, −2.3636 ± *i* 185.8, −38.926, −17.907 ± *i* 24.421, **0.14983 ± *i* 6.2653**, −2.9177, −20.218 & the corresponding response is as shown in the Fig. 29. As the system is having a positive eigen value, the same is reflected in the response which shows that the system moves towards instability.

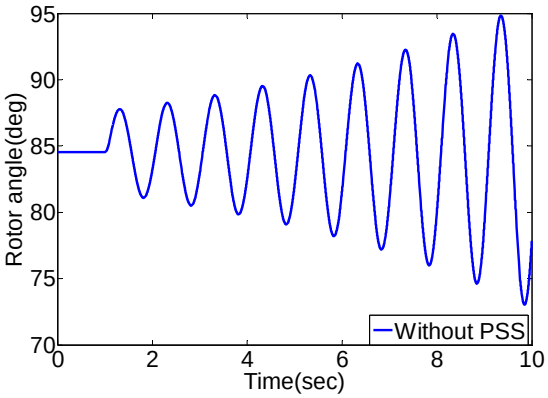

Fig. 29 : Response of Rotor angle without PSS vs. time

The eigen value analysis is also performed for the model 2.2 with the CPSS & the values are obtained as −3.4512 ± *i* 568.15, −499.2, −2.3705 ± *i* 185.74, −101.11, −38.893, −16.692 ± *i* 26.214, −20.219, −0.52381 ± *i* 6.058, −2.9051, −0.10033 & the corresponding response is as shown in the Fig. 30.

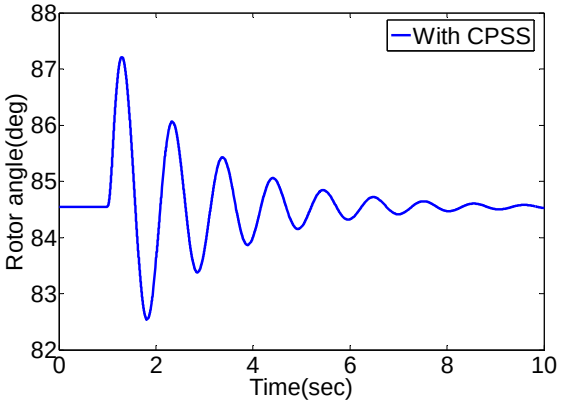

Fig. 30 : Response of Rotor angle with CPSS

The eigen value analysis is also performed for the model 2.2 with the RPSS & the values are obtained as −14872 ± *i* 8367.8, −7232.1 ± *i* 2642, −437.38 ± *i* 221.2, −3.4771 ± *i* 568.14, −406.29, −499.18, −2.3901 ± *i* 185.91, −38.972, −14.603 ± *i* 21.991, −3.2537 ± *i* 6.5439, −2.8128, −20.213 & the corresponding response is as shown in the Fig. 31.

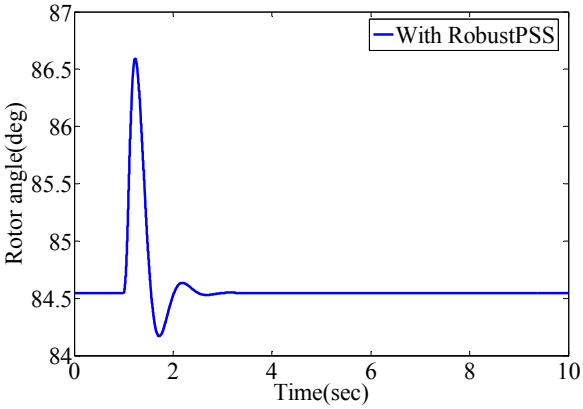

Fig. 31 : Response of Rotor angle with Robust PSS

3.2.5 Simulation results & discussions

Simulations are performed using the developed simulink model shown in the Figs. 27 & 28 for a period of 10 secs with the designed CPSS & RPSS and the results are observed, which are presented in Figs. 32 - 35 respectively. The non-linear simulations are performed, for extreme fault conditions, using simulink to test the efficiency of the designed controller. 4 different types of faults were considered as case A, B, C & D respectively.

Case A : $P_g = 0.9$, $V_{ref} = 1.0$ & $T_m = 1.1$(for 0.1 sec).

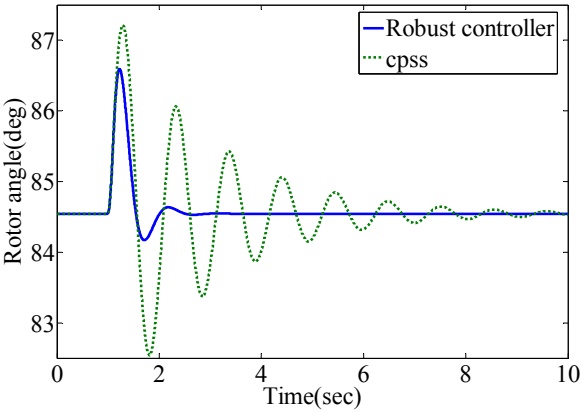

Fig. 32 : Plot of rotor angle in deg vs. time

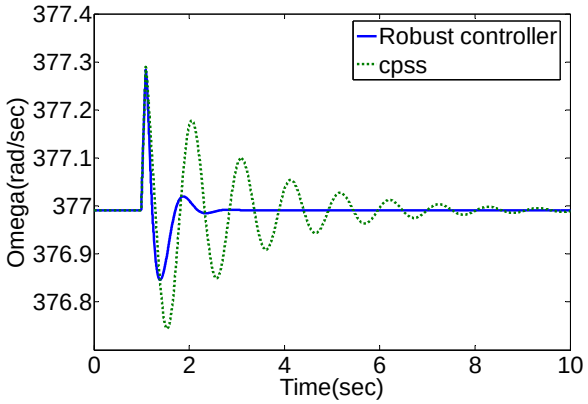

Fig. 33 : Plot of omega in rad / sec vs. time

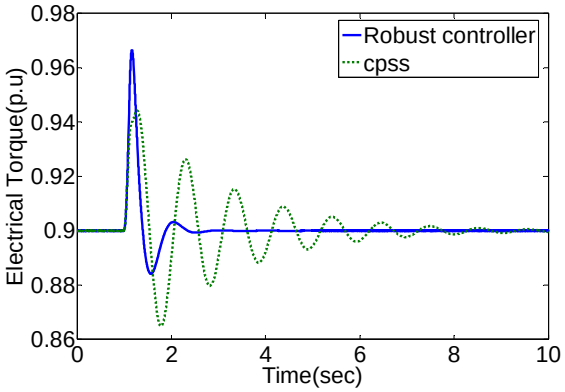

Fig. 34 : Variation of electric torque vs. time

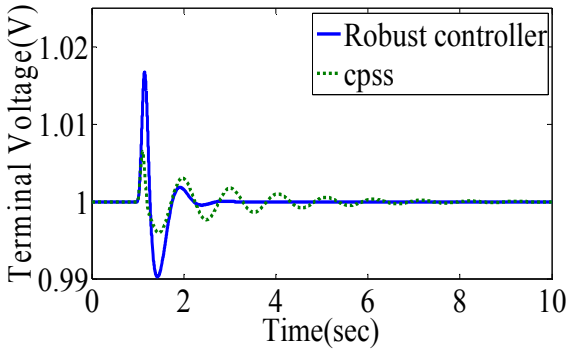

Fig. 35 : Variation of terminal voltage vs. time

Parameters	Settling time (secs)	
	CPSS	RPSS
Rotor angle	12	3
Omega	11	3
Torque	10.5	3
Voltage	10	3

Table 2: Quantitative results of the settling times of different parameters with CPSS & RPSS for the model 2.2.

From the Figs. 32 to 35, it can be clearly seen that system with RPSS, the settling time and deviation in magnitudes during transients are insignificant & consistent when compared to the CPSS. The quantitative results of the comparison of the settling times of the various parameters with CPSS & RPSS is shown in the table 2.

In addition to the above fault as mentioned in case A, three more cases are simulated, namely

Case B: $P_g = 1.4,\ V_{ref} = 1.0,\ T_m = 1.1 (\text{for } 0.1\,s)$

Case C: $P_g = 0.9,\ V_{ref} = 1.1\ (\text{for } 0.1s),\ T_m = 1.0$

Case D: Three phase fault for 0.08 sec.

The simulation results of all these cases are similar to the results shown for case A.

For justification of robustness, the following 3 cases with different generated powers & a simultaneous 3-ϕ fault are considered, namely,

Case 1 : $P_g = 0.9$ & three phase fault for 0.1 sec.

Case 2 : $P_g = 0.5$ & three phase fault for 0.1 sec.

Case 3 : $P_g = 1.4$ & three phase fault for 0.1sec.

The simulation results corresponding to the above 4 cases are shown in the Figs. 36 to 41 respectively. The results shown in Figs. 36, 38 & 40 correspond to the system with RPSS while the results shown in Figs. 37, 39, & 41 respectively correspond to the system with CPSS.

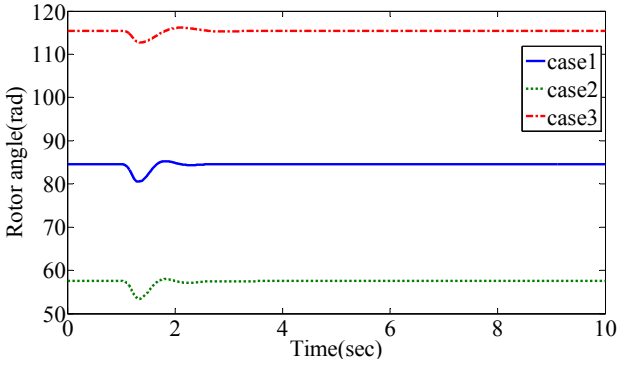

Fig. 36 : Plot of rotor angle with robust controller vs. time

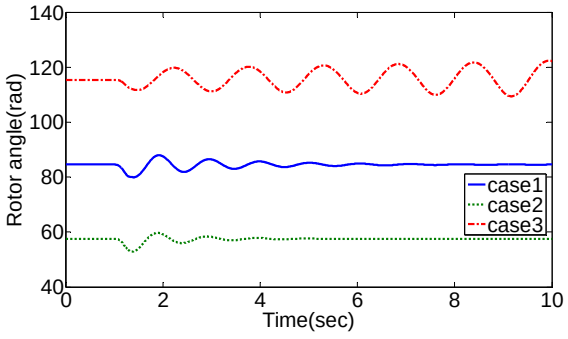

Fig. 37 : Plot of rotor angle with CPSS vs. time

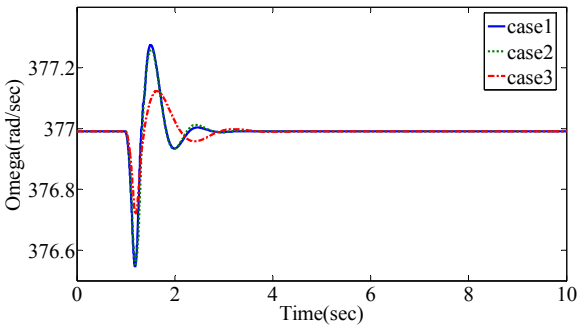

Fig. 38 : Plot of omega with robust controller vs. time

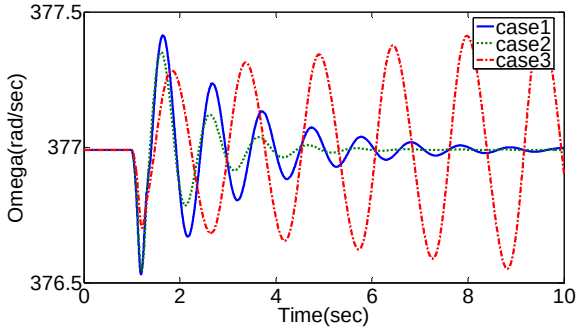

Fig. 39 : Plot of omega with CPSS vs. time

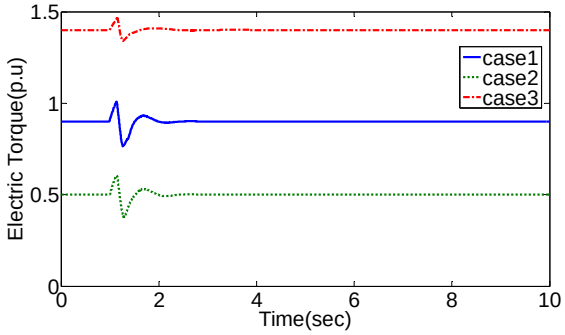

Fig. 40 : Plot of electric torque with robust controller

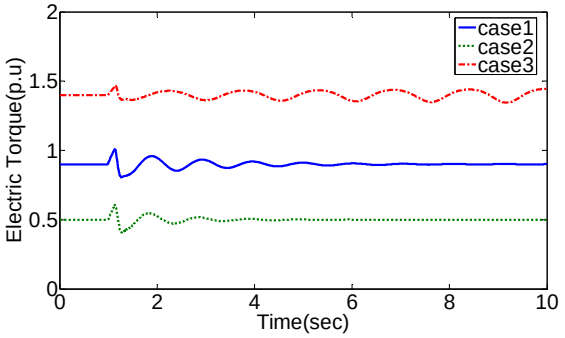

Fig. 41 : Plot of electric torque with CPSS vs. time

From the above simulation results shown in the Figs. 36 - 41, it can be very clearly seen that the system with RPSS provides robustness, i.e., the variations in magnitudes and the settling times are almost independent of the type and magnitude of faults, while the system with CPSS fails to provide robustness as the settling time depends upon the type of faults, also the response characteristics for various parameters settle at a faster rate compared to the CPSS case, thus RPSS provides excellent damping. It is also observed that in Figs. 37, 39, 41, that for the case 3, the system with CPSS becomes unstable.

4. Conclusions

A systematic approach to design the power system stabilizers using Glover-McFarlane's loop shaping procedure (H_∞ robust control) was presented in this research paper. Two power systems models, viz., model 1.1 & 2.2 were considered and these models were used to develop the controller for stabilization purposes in both the cases. The guidance to select the weighting functions for the H_∞ robust control was also presented. Two cases was considered, control with CPSS & control with RPSS. Similulink model was developed & the simulations were performed for a period of 10 secs. Response curves of torque, omega, terminal voltage & delta were observed. Simulation results demonstrate the good damping performance of the designed RPSS. Comparisons of the robust controller with the CPSS show that H_∞ controller can achieve excellent robustness, while the design procedure used is much simpler. Collectively, these results show that the loop shaping controller provides faster settling times, less ringing oscillations (overshoots & undershoots) & good stabilization. The eigen value analysis for the models 1.1 & 2.2 with CPSS & RPSS was also carried out. It was observed that the eigen values shows better stabilization with RPSS compared to CPSS. The settling time and deviation in magnitudes during transients are comparatively insignificant with the introduction of the RPSS in loop with the plant. By the method presented in this paper, the efficiency, performance and reliability of the power system increases as the robustness factor comes into picture using the H_∞ control. Model 1.1 is normally used for multi-machine modelling as the required data is available in most of the multi-machine systems, while the model 2.2 can be used for SMIB systems as it is difficult to obtain the detailed data for the model 2.2 in case of multi-machine systems. The above procedure can be applied to multi-machine power system to design the robust controller to take care of the intra-area oscillations under perturbed conditions. Also, the method adopted in this paper can be used for

power system stabilization & implementation in real time using dSpace interfacing cards.

NOMENCLATURE

AVR	Automatic Voltage Regulator
CPSS	Conventional Power System Stabilizers
MIMO	Multiple Input Multiple Output
PSS	Power System Stabilizers
RPSS	Robust Power System Stabilizers
SISO	Single Input Single Output
SMIB	Single Machine Infinite Bus
SSV	Structured Singular Value

REFERENCES

[1] D.C. MacFarlane and K. Glover, "A loop shaping design procedure using H∞ synthesis", Vol. AC-37: *IEEE Trans. Auto. Control.,* pp. 759–769, 1992.

[2] J. C. Doyle, B. A. Francis, and A. R. Tannenbaum "Feedback control theory", *Macmillan Press*, New York, 1992.

[3] J. M. Maciejowski, "Multivariable feedback design", *Addison-Wesley publishing company*, Singapore.

[4] J. C. Zhou, J. C. Doyle, and K. Glover, "Robust and optimal control", *Prentice Hall Inc.*, New Jersey, USA, 1996.

[5] Geir E. Dullerud and Fernando Paganini, "A course in Robust Control Theory", *Springer*, 1999.

[6] Tprkel Glad and Lennart Ljung, "Control Theory: Multivariable and Nonlinear Methods", *Taylor and Francis*, U.K.

[7] Benzamin C.kuo, "Automatic control systems", *Prentice-Hall of India*, New Delhi, 2001.

[8] Anderson P.M and Fouad A.A., "Power system control and stability", *Iowa state university press*, Ames, 1977.

[9] Padiyar. K.R., "Power system Dynamics Stability and Control", *B.S. publications*, Second Edn., 2002.

[10] P. Kundur, "Power System Stability and Control", *McGraw-Hill*, New York, 1993.

[11] Matlab Help Documentation Release 12, *Mathworks*, USA.

[12] Jie Feng and Malcolm.c,Smith, "When is a controller in the sense of H∞ loop shaping ?" *Proc. of the IEEE Trans. on Automatic Contr.*, Vol. 40, No. 12, Dec. 1995.

[13] Papageorgiou. G., & Glover K., "H_∞ loop-shaping : Why is it a sensible procedure for designing robust flight controllers ?", *Proc. of the AIAA conference on guidance, navigation and control*, USA, 1996.

[14] McFarlane, D., & Glover, K., "Robust controller design using normalized coprime factor plant descriptions", *Lecture notes in control and information sciences*, Vol. 138, 1st ed., Berlin: Springer, 1990.

[15] Hyde, R. A., "H_∞ aerospace control design — A VSTOL flight application. In Advances in industrial control series", *Springer*, Berlin, 1995.

[16] Chuanjiang Zhu, Mustafa KhammashVijay Vittal, Fellow, Wenzheng Qiu, "Robust Power System stabilizer Design Using H_∞ Loop Shaping Approach" *Proc. of the IEEE Trans. on Power Systems*, Vol. 18, No. 2, pp. 810-819. May, 2003.

Jayapal. R. obtained B.E. in Electrical Engineering and Masters degree in power systems from Bangalore University in the years 1984 and 1986 respectively. Presently, working towards doctoral degree in Electrical Engg. In the field of power systems in the prestigious Visvesvaraya Technological University, India. He has been working as a faculty in the department of electrical and electronics engineering, RVCE, Bangalore, since 1986. He is a life member of ISTE. He has published a number of papers in various national & international conferences, journals. His area of interests are power systems, Control systems, Power electronics, Power systems stability & its allied branches.

Dr. J.K. Mendiratta obtained Doctoral degree in Power and Control Systems from IIT, Delhi. He received Master degree in Electrical Machines & Control from Roorkee University (now IIT-Roorkee) and B.E. in Electrical Engineering from Roorkee University (now IIT-Roorkee). He is a Senior Member-IEEE-USA. He has worked at design and development centre at BHEL, India for 32 years. He has published a number of papers in various national & international conferences, journals. He has worked as Professor in the department of electronics and communication engineering, RVCE, Bangalore for 5 years. Presently he is working as professor in the department of Information Science engineering, CMRIT, Bangalore. He has published a number of papers in various national & international conferences, journals.